The need for de-aliasing in a Chebyshev pseudo-spectral method

Markus Uhlmann

Potsdam Institut für Klimafolgenforschung, D-14412 Potsdam
uhlmann@pik-potsdam.de

(March 2000)

Abstract

In the present report, we attempt to estimate whether the computational overhead due to the explicit removal of Chebyshev-pseudo-spectral-induced aliasing errors is necessary in a DNS of plane channel flow. We first recall the origin of aliasing errors in a Chebyshev method before turning to results from different test cases: analytical; transition to turbulence; fully-developed turbulence.

Our results indicate that corrective action can slightly improve the quality of the solution in situations where the resolution is marginal. We do not find conclusive evidence that supports the use of the de-aliasing strategy under non-marginal conditions.

1. Introduction

In the past, various authors have investigated the importance of aliasing errors in Fourier-based pseudo-spectral methods for direct numerical simulation (DNS) of turbulent flows (cf. Canuto, Hussaini, Quarteroni & Zang (1988) for a survey). The explicit removal of such errors has become common practice in numerical turbulence studies since the recognition of the 2/3-rule by Orszag (1971) and the introduction of the relatively low-cost combination of phase-shifts and truncation by Rogallo (1981). However, the importance of aliasing errors when using Chebyshev polynomial expansions instead of Fourier series has – to my knowledge – not been addressed in detail in the literature. While Canuto *et al.* (1988) briefly describe the existence and possible removal of aliasing errors in Chebyshev pseudo-spectral methods, actual simulations of the Navier-Stokes equations have apparently been commonly performed without resorting to such corrections (e.g. Kim *et al.* (1987), Krist & Zang (1987), Hill & Ball (1999)).

In the present report, we attempt to estimate whether the computational overhead due to the explicit removal of Chebyshev-induced aliasing errors is necessary (i.e. paying off in terms of efficiency) in a DNS of plane channel flow. We first recall the origin of aliasing errors in a Chebyshev method before turning to results from different test cases: analytical; transition to turbulence; fully-developed turbulence.

Our present results indicate that corrective action can slightly improve the quality of the solution in situations where the resolution is marginal. We do not find conclusive evidence that supports the use of the de-aliasing strategy under non-marginal conditions.

2. Aliasing errors

In a discrete representation of continuous data the frequency content beyond the critical (Nyquist) frequency is in general misinterpreted. One speaks of 'aliasing' when supercritical frequencies are erroneously attributed to lower frequencies within the resolved range. In a numerical approximation of partial differential equations, such high frequency content of the solution is being generated by non-linear terms. In the case of the Navier-Stokes equations, these (convective) terms are of quadratic order. Let us consider a Chebyshev pseudo-spectral method (i.e. one where the product is evaluated in physical space and fast transforms are used to shuttle to and from spectral space) for computing a product between two functions u, v. The Nth order truncated Chebyshev expansion reads:

$$\left.\begin{array}{rcl} U_j &=& \displaystyle\sum_{m=0}^{N} \hat{u}_m\, T_m(x_j) \\ V_j &=& \displaystyle\sum_{n=0}^{N} \hat{v}_n\, T_n(x_j) \end{array}\right. \qquad 0 \le j \le N \quad , \tag{2.1}$$

where for the Gauss-Lobatto grid:

$$x_j = \cos(\pi j/N)\,, \qquad T_m(x_j) = \cos(m\pi j/N)\,. \tag{2.2}$$

The Chebyshev coefficients of the non-linear term $Z_j = U_j \cdot V_j$ read

$$\hat{z}_k = \frac{1}{\gamma_k} \sum_{j=0}^{N} Z_j\, T_k(x_j)\, w_j \quad , \tag{2.3}$$

with the following weights and normalization factors

$$w_j = \begin{cases} \pi/2N & j=0,N \\ \pi/N & 1 \le j \le N-1 \end{cases} \qquad \gamma_k = \begin{cases} \pi & k=0,N \\ \pi/2 & 1 \le k \le N-1 \end{cases} \tag{2.4}$$

Substituting (2.1) into (2.3) leads to:

$$\begin{aligned} \hat{z}_k &= \frac{1}{\gamma_k} \sum_{j=0}^{N} \sum_{m=0}^{N} \sum_{n=0}^{N} \hat{u}_m \, T_m(x_j) \, \hat{v}_n \, T_n(x_j) \, T_k(x_j) \, w_j \\ &= \frac{1}{4\gamma_k} \sum_{j=0}^{N} w_j \sum_{m=0}^{N} \sum_{n=0}^{N} \hat{u}_m \, \hat{v}_n \, \{\cos(a_j(m-n+k)) + \cos(a_j(m-n-k)) \\ &\quad + \cos(a_j(m+n+k)) + \cos(a_j(m+n-k))\} \quad , \end{aligned} \tag{2.5}$$

where $a_j = \pi j/N$. The discrete orthogonality relation for Chebyshev polynomials reads:

$$\frac{1}{N+1} \sum_{j=0}^{N} T_p(x_j) = \frac{1}{N+1} \sum_{j=0}^{N} \cos(p\pi j/N) = \begin{cases} 1 & \text{if} \quad p = 2Nm \quad m = 0, \pm 1, \ldots \\ 0 & \text{else} \end{cases} \tag{2.6}$$

Therefore (2.5) becomes

$$\begin{aligned} \hat{z}_k = \frac{\pi}{4\gamma_k} \Bigg\{ & \Bigg[\sum_{m-n+k=0} \hat{u}_m \, \hat{v}_n + \sum_{m-n-k=0} \hat{u}_m \, \hat{v}_n + \sum_{m+n-k=0} \hat{u}_m \, \hat{v}_n + \sum_{m+n+k=0} \hat{u}_m \, \hat{v}_n \Bigg] \\ + & \Bigg[\sum_{m-n+k=2Np} \hat{u}_m \, \hat{v}_n + \sum_{m-n-k=2Np} \hat{u}_m \, \hat{v}_n + \sum_{m+n-k=2Np} \hat{u}_m \, \hat{v}_n + \sum_{m+n+k=2Np} \hat{u}_m \, \hat{v}_n \Bigg] \Bigg\} \end{aligned} \tag{2.7}$$

(where $p = 0, \pm 1, \ldots$). The terms in the second pair of square brackets are aliasing errors. In order to have an Nth order representation that is free of such aliasing errors, a total number of $M > N$ modes can be chosen for the basic expansion, setting high wavenumber coefficients to zero. What is the minimum number M which fulfills that requirement? Considering the very last sum which under these conditions passes over all indices for which $m+n+k = 2M$, the worst case is when $m = n = N$ (beyond which all $\hat{u}_m$, $\hat{v}_n$ are zero). We want the first alias-affected wavenumber to lie just outside the 'useful' range, therefore $k = N+1$, which in turn leads to the following condition:

$$M \ge \frac{3(N+1)}{2} - 1 \quad . \tag{2.8}$$

It is obvious that de-aliasing can be achieved as in Fourier pseudo-spectral methods by the 3/2-rule (cf. also (Canuto *et al.* 1988, p.86)), i.e. $M = 3(N+1)/2 - 1$ collocation points are chosen in physical space while only N Chebyshev modes are retained for computation in spectral space and the remaining coefficients are removed/padded with zeroes during the transformation steps.

After having computed the product in physical space, further operations are performed using the spectral coefficients, e.g. the computation of a derivative $z_{,x} = (u\,v)_{,x}$. The Chebyshev derivative involves the following operations:

$$Z'(x_j) = \sum_{m=0}^{N} \hat{z}_m^{(1)} \, T_m(x_j) \quad , \tag{2.9}$$

where the derivative coefficients in Chebyshev space read (Canuto *et al.* (1988)):

$$\hat{z}^{(1)}_m = \frac{2}{c_m} \sum_{\substack{p=m+1 \\ p+m \text{ odd}}}^{N} p\,\hat{z}_p\,, \qquad c_m = \begin{cases} 2 & \text{if } m = 0 \\ 1 & \text{else} \end{cases} \quad . \tag{2.10}$$

The last formula shows that derivatives are given by a recurrence relation in decreasing order, which implies that truncation and differentiation do not commute (Canuto *et al.* 1988, p.68). Therefore, when using the 3/2-rule for de-aliasing, truncation should be performed immediately after passing data to spectral space in order to prevent the alias-affected coefficents with $N+1 \leq k \leq M$ from affecting the 'useful range' $0 \leq k \leq N$. Alternatively, a total number of $\widetilde{M} = 2\,N$ modes could be used ('4/2-rule', cf. Orszag (1971)) in order to obtain a full alias-free length $\widetilde{M}$ and then truncating only at the end of each step, just before re-transforming to physical space. For reasons of computational overhead, we will only consider the 3/2-rule in the following.

3. Analytical test

We consider the Chebyshev pseudo-spectral computation of the function

$$f(x) = (u^2)_{,x}\,, \qquad u(x) = \sin(10 \cdot 22/19\pi\,x)\,, \qquad 0 \leq x \leq 2 \quad . \tag{3.1}$$

Convergence is measured by the square norm of the error normalized with the r.m.s. value of $f(x)$ for different numbers of modes N in the 'useful range', i.e. $N = M$ for the aliased scheme and $N = (M+1)2/3 - 1$ for the de-aliased scheme. The corresponding diagram is shown in figure 1 (a), where both methods are seen to lead to similar errors. In fact, the above measure of the error contains two contributions:

(i) the aliasing (or 'interpolation') error due to the projection of the basic function $u(x)$ upon the truncated Chebyshev series:

$$\hat{u}_k = \widetilde{u}_k + \underbrace{\sum_{\substack{j=2mN\pm k \\ j>N}} \widetilde{u}_j}_{\text{interpolation error}} \quad , \tag{3.2}$$

(where $\widetilde{u}_k$ is a mode of the *continuous* Chebyshev transform, cf. (Canuto *et al.* 1988, p.68));

(ii) the aliasing error due to the pseudo-spectral computation of the non-linear term $u^2(x)$ as in equation (2.7), i.e. the error associated with the discrete representation of the high-frequency content generated by squaring the signal.

An alternative measure of the error can be defined which singles out the second contribution (ii) only: the error of the numerical solution F with respect to the frequency content of the exact solution lying within the respective 'useful range', i.e.:

$$\text{error} = \sqrt{\frac{1}{N+1} \sum_{i=0}^{N} (F(x_i) - f_N(x_i))^2} \quad , \tag{3.3}$$

where the N-mode low-pass filtered function is given by:

$$f_N(x_j) = \sum_{k=0}^{N} \hat{\hat{f}}_k\, T_k(x_j)\,, \qquad \hat{\hat{f}}_k = \frac{1}{\gamma_k} \sum_{j=0}^{K} f(x_j)\, T_k(x_j)\, w_j \quad , \tag{3.4}$$

and K is a large finite number of modes in practice (here: $K = 512$). Figure 1 (b) shows the convergence measured according to (3.3); the effect of de-aliasing is visible: as expected, the limited range of wavenumbers N is better represented than with aliasing errors for intermediate wavenumbers. However, since in an actual simulation both errors (i) and (ii) are simulataneously present, the effect of the de-aliasing procedure gets blurred as we will observe in the following more realistic test cases.

4. Transition

In this section we present results from the simulation of the early stages of transition to turbulence in plane channel flow. The numerical scheme is based upon the method of Kim, Moin & Moser (1987), i.e. truncated Fourier series in the spanwise (z) and streamwise (x) coordinate direction and a Chebyshev polynomial representation in the wall-normal (y) direction is used. Non-linear terms are evaluated pseudo-spectrally, performing de-aliasing according to the 3/2-rule consistently in the (x, z) Fourier plane. It is our present purpose to evaluate the need for de-aliasing in the remaining direction under realistic circumstances and we will therefore present results that have been obtained with and without de-aliasing of the Chebyshev modes according to the method outlined in §1. For completeness, let us mention that the time integration is semi-implicit based upon a three-step Runge-Kutta method and an implicit solution of the viscous problem. In what follows, the time step was determined according to the linear CFL stability criterion of the method; therefore, the temporal discretization error is not minimized and generally interferes with the spatial error.

The present test case is similar to one of the cases considered by Krist & Zang (1987) (cf. also Zang, Krist & Hussaini (1989)) in their resolution study. We consider the secondary instability of Poiseuille flow at $Re = U_0 h/\nu = 8000$ which is linearly unstable to two-dimensional normal mode perturbations in a narrow band of streamwise wavenumbers around $\alpha h = 1$. The linear eigenfunction has been computed by a numerical eigensystem analysis of the Orr-Sommerfeld equations using 400 sixth order B-splines. The initial field has been assigned to our two evolution variables $\varphi = \nabla^2 v$ and $\omega_y = u_{,z} - w_{,x}$ in the following manner:

$$\begin{aligned} \varphi(x, y, z, t_0) &= A_{2D}\, \varphi_{2D}(x, y) + A_{3D}\, e^{I\phi(x,z)2\pi} \\ \omega_y(x, y, z, t_0) &= 0 \quad , \end{aligned} \tag{4.1}$$

where $A_{2D} = 0.01$ is the amplitude of the linear 2D perturbation given by φ_{2D} and $A_{3D} = 2 \times 10^{-4}$ is the amplitude of supplementary 3D background noise whose phase angle is determined by the random variable $0 \le \phi(x, z) \le 1$. Since the $(k_x = 0, k_z = 0)$-mode is resolved separately, the Poiseuille base flow is directly assigned to the respective "primitive" variable

$$u_{00}(y, t_0) = U_0 \cdot y\,(2 - y)\,, \qquad 0 \le y \le 2 \quad . \tag{4.2}$$

Note that the (random) initial field was generated only once at the lowest wall-normal resolution and then adapted for subsequent runs at higher resolution by filling up the high wavenumbers with zeroes. Throughout this section, 96×32 Fourier modes (before de-aliasing) were utilized while the box size measured $L_x/h = 2\pi$ and $L_z/h = 0.833$. The number of Chebyshev modes in the 'useful range' was varied from $N_y = 33$ up to $N_y = 97$ ($M_y = 145$).

Figure 2 shows the spectrum of Chebyshev coefficients of the initial 2D perturbation which is essentially captured by the first 30-40 modes. As a basic test, we have computed

method	$\Im(c)$
'exact'	$2.66441E-3$
$N_y = 33$ aliased	$2.63282E-3$
$N_y = 49$ aliased	$2.63259E-3$
$N_y = 97$ de-aliased	$2.63259E-3$

TABLE 1. Effect of vertical resolution on the growth rate of the least stable two-dimensional perturbation at $Re = 8000$. The 'exact' result has been obtained by numerical solution of the Orr-Sommerfeldt equation using 400 B-splines of order 6 (cf. also Krist & Zang (1987)).

the growth rate of the linear perturbation by means of the full non-linear code†. Table 1 shows the results for different wall-normal resolutions. When using 33 aliased Chebyshev modes, the temporal growth rate of the energy of the fundamental streamwise harmonic is predicted within 10^{-4} accuracy relative to the numerical result at $N_y = 97$ (de-aliased). Note that the 'exact' linear result differs by about 1% which we attribute to the temporal integration error.

Figure 3 again shows the evolution of the kinetic energy of that same harmonic, but starting from the finite amplitude perturbation given by (4.1). Note that under these circumstances rapid transition sets in at $t \approx 60h/U_0$, shortly beyond the time interval presently under consideration. The various curves of the figure – corresponding to different Chebyshev grids, aliased and de-aliased – can barely be distinguished.

Isocontours of the spanwise vorticity in the (x, y)-plane are plotted in figures 4-8 at $t = 20h/U_0$ and $t = 55h/U_0$. At both stages of the evolution, small differences between the $N_y = 33$ and the more highly resolved fields ($N_y = 49$, $N_y = 97$) can be discerned. The deviations are slightly more pronounced when no de-aliasing is performed. However, at no stage important oscillations are observed as is the case when the Fourier directions are under-resolved or marginally resolved *and* aliased (cf. Krist & Zang (1987)).

5. Fully developed turbulence

We consider the evolution of the flowfield in the plane channel configuration of §4 but in the regime of fully developed turbulent motion at a Reynolds number of $Re = 3250$. The box size is chosen as $L_x = 8.49h$ and $L_z = 3.31h$; the resolution is 192×128 modes in the Fourier directions (before de-aliasing) and $N_y = 97$ Chebyshev modes in the 'useful range'. The initial field is taken from a simulation without de-aliasing in the wall-normal direction and was spectrally up-sampled for continuation with de-aliasing.

Figure 9 shows the temporal evolution of the plane-averaged friction factor c_f. It can be observed that the aliased and de-aliased results start to differ noticeably after an elapsed time of about $15h/U_0$ which corresponds to 150 viscous time units ($t^+ = tu_\tau^2/\nu$ where u_τ is the friction velocity).

The wall-normal spectra of component energy and enstrophy,

$$E_{\alpha\alpha}(k_y) = \int\int \hat{u}_\alpha(k_x, k_y, k_z)\, \hat{u}^*_\alpha(k_x, k_y, k_z) \mathrm{d}k_x \mathrm{d}k_z \tag{5.1}$$

$$W_{\alpha\alpha}(k_y) = \int\int \hat{\omega}_\alpha(k_x, k_y, k_z)\, \hat{\omega}^*_\alpha(k_x, k_y, k_z) \mathrm{d}k_x \mathrm{d}k_z \quad , \tag{5.2}$$

where $\vec{\omega} = \nabla \times \vec{u}$ is the vorticity (no implied summation for greek indices; asterisk denotes

† For this test only, the initial amplitudes were set to: $A_{2D} = 10^{-5}$ and $A_{3D} = 0$.

complex conjugation) is shown in figure 10 after an elapsed time of $2h/U_0$. The slight 'pile-up' of energy in high-wavenumber coefficients that occurs in the aliased simulation is absent when de-aliasing is employed. Figures 11 and 12 show isocontours of spanwise and streamwise vorticity in (x, y)- and (z, y)-planes respectively. No differences between results from the two schemes are visible at this stage of the simulation.

At the later stage ($t = 40h/U_0$), the spectral distribution of energy and enstrophy shows a very similar character as earlier on (figure 13). By now, however, the aliased and de-aliased flowfields have taken a slightly different shape from one another, as can be deduced from the contourplots in figures 14 and 15 and had been indicated by the slow divergence of the skin friction mentioned above. On the other hand, this is no surprise considering the disordered character of the turbulent motion which allows for a divergence of only slightly perturbed states.

6. Conclusion

Our present computations seem to lead to a conclusion that is similar to the one reached in (Krist & Zang 1987, p.5) with respect to de-aliasing in Fourier spectral methods:

> "Both aliased and de-aliased calculations are valid until they lose resolution; the aliased calculation loses resolution slightly sooner than a de-aliased calculation with an equal number of active modes."

It is therefore not established that the additional effort stemming from the one-third increase in collocation points according to the 3/2-rule pays off in a realistic, well-resolved simulation.

REFERENCES

Canuto, C., Hussaini, M., Quarteroni, A. & Zang, T. 1988 *Spectral methods in fluid dynamics*. Springer.

Hill, R. & Ball, K. 1999 Parallel implementation of a Fourier-Chebyshev collocation method for incompressible fluid flow and heat transfer. *Num. Heat Transfer, Part B* **36**, 309–329.

Kim, J., Moin, P. & Moser, R. 1987 Turbulence statistics in a fully developed channel flow at low Reynolds number. *J. Fluid Mech.* **177**, 133–166.

Krist, S. & Zang, T. 1987 Numerical simulation of channel flow transition: Resolution requirements and structure of hairpin vortex. *Tech. Rep.* 2667. NASA.

Orszag, S. 1971 On the elimination of aliasing in finite-difference schemes by filtering high-wavenumber components. *J. Atmos. Sci.* **28**, 1074.

Rogallo, R. 1981 Numerical experiments in homogeneous turbulence. *Tech. Rep.* TM 81315. NASA.

Zang, T., Krist, S. & Hussaini, M. 1989 Resolution requirements for numerical simulations of transition. *J. Sci. Comp.* **4** (2), 197–217.

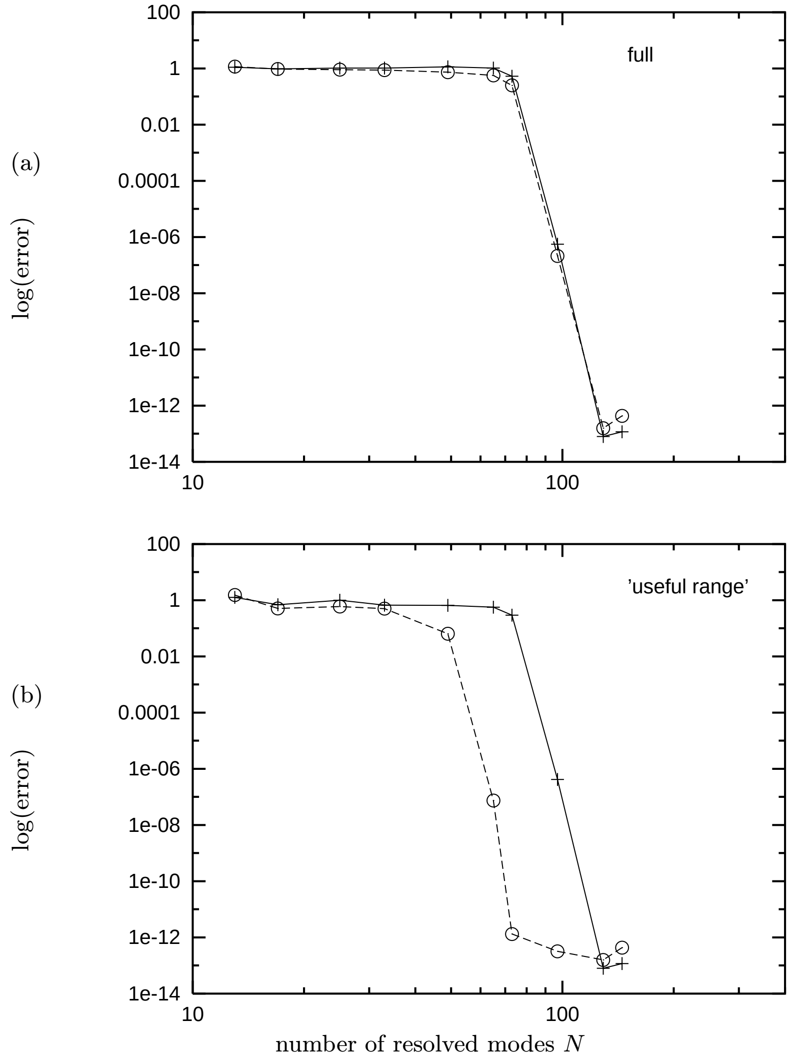

FIGURE 1. Square norm of the pointwise error of the Chebyshev pseudo-spectral calculation of the non-linear term $(u^2)_{,x}$ for $u(x) = \sin(10 \cdot 22/19\pi\, x)$ $(0 \leq x \leq 2)$. (a) Error with respect to the full analytical solution. (b) Error relative to the exact solution low-pass filtered with the number of Chebyshev modes N_y as threshold, i.e. the part of the solution that contains only contributions from the 'useful range' of the spectrum. $+$, aliased Chebyshev modes; $\circ$, de-aliased according to the 3/2-rule.

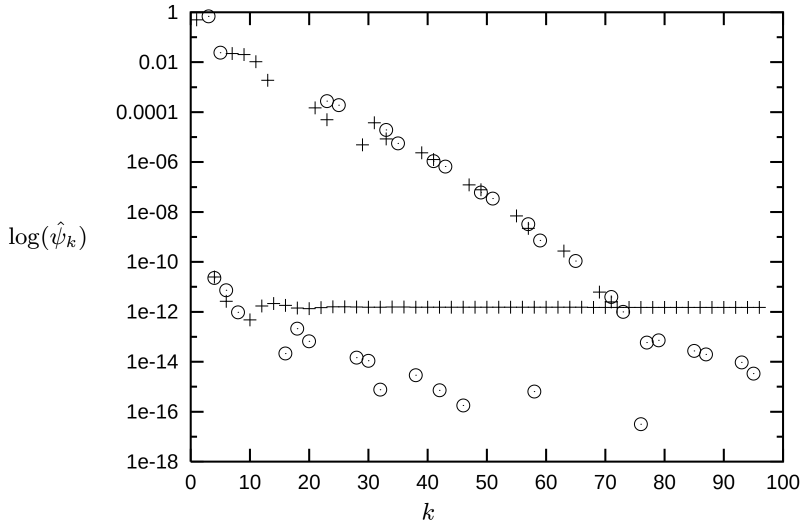

FIGURE 2. Decay of the Chebyshev coefficients of the least stable two-dimensional eigenfunction of the streamfunction $\psi_y(y)$ (where $\psi(x,y,t_0) = \psi_y(y)\, e^{i\alpha(x-ct_0)}$) obtained by linear stability analysis at $Re = 8000$: $+$, real part; $\circ$, imaginary part.

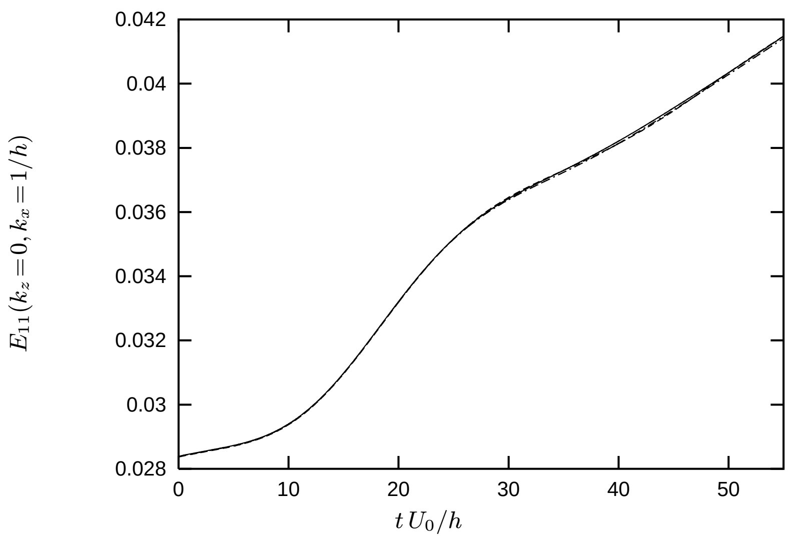

FIGURE 3. Temporal growth of the kinetic energy of the mode with $(k_x=1, k_z=0)$ during the non-linear evolution from finite initial value at $Re = 8000$: ——— , $N_y = 97$ de-aliased; - - - - , $N_y = 33$ aliased; —·— , $N_y = 33$ de-aliased.

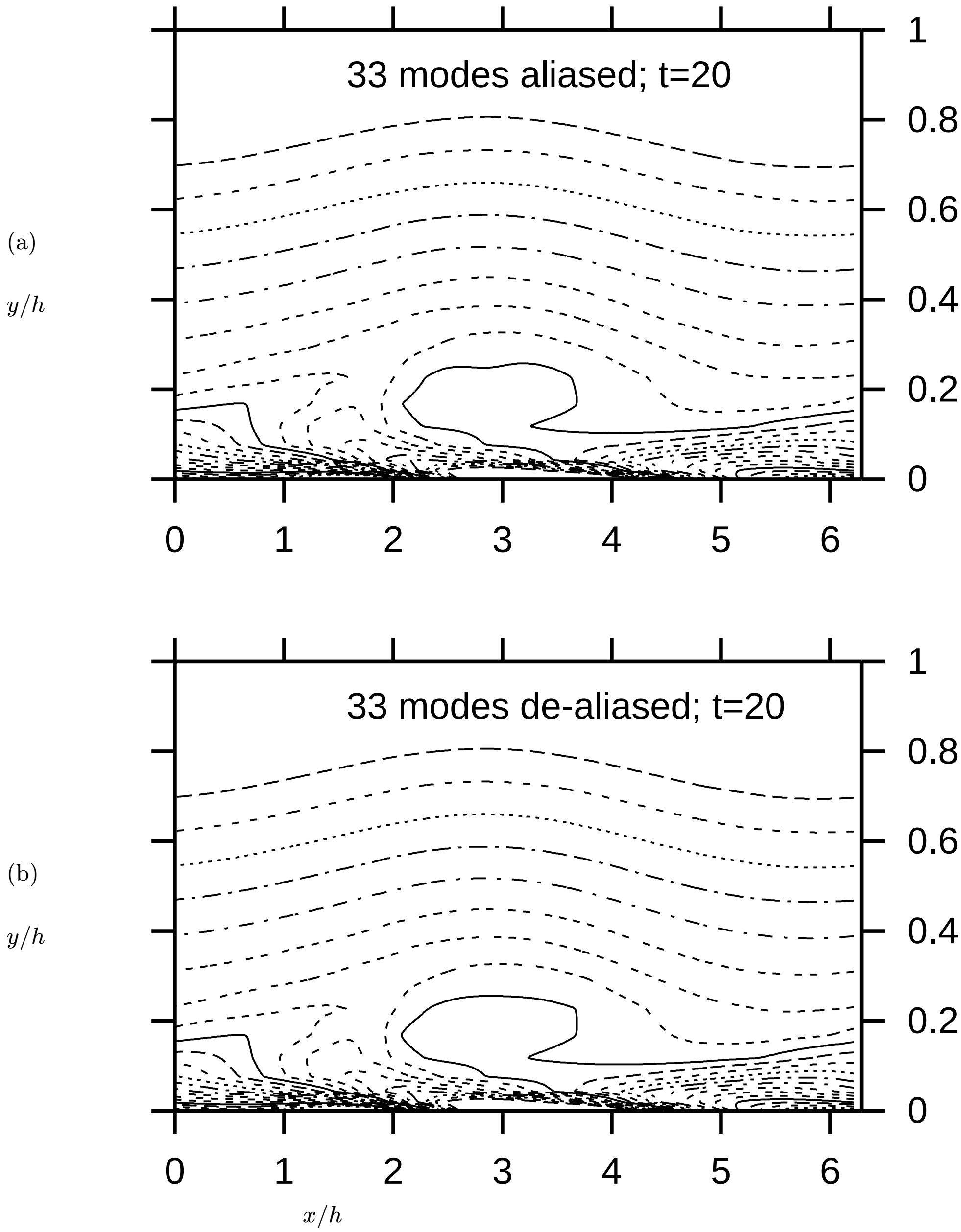

FIGURE 4. Isocontours of spanwise vorticity at values $(-3.5 : .15 : -.5)$ at $t = 20\,h/U_0$ when initialising with the most unstable 2d linear eigenfunction at $Re = 8000$ and using $96 \times 33 \times 32$ modes: (a) aliased Chebyshev modes, (b) de-aliased according to the 3/2-rule.

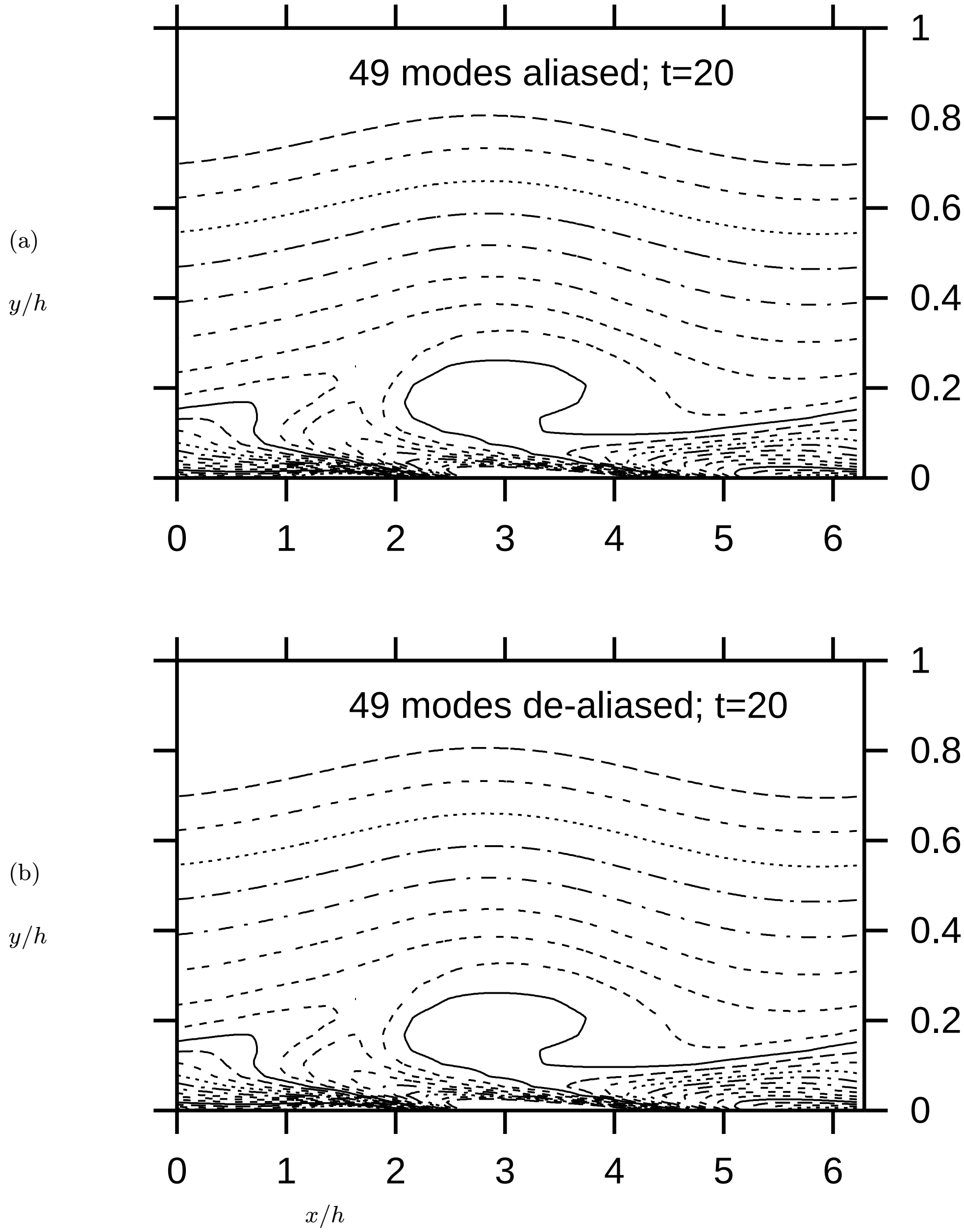

FIGURE 5. Isocontours of spanwise vorticity at values $(-3.5 : .15 : -.5)$ at $t = 20\,h/U_0$ when initialising with the most unstable 2d linear eigenfunction at $Re = 8000$ and using $96 \times 49 \times 32$ modes: (a) aliased Chebyshev modes, (b) de-aliased according to the 3/2-rule.

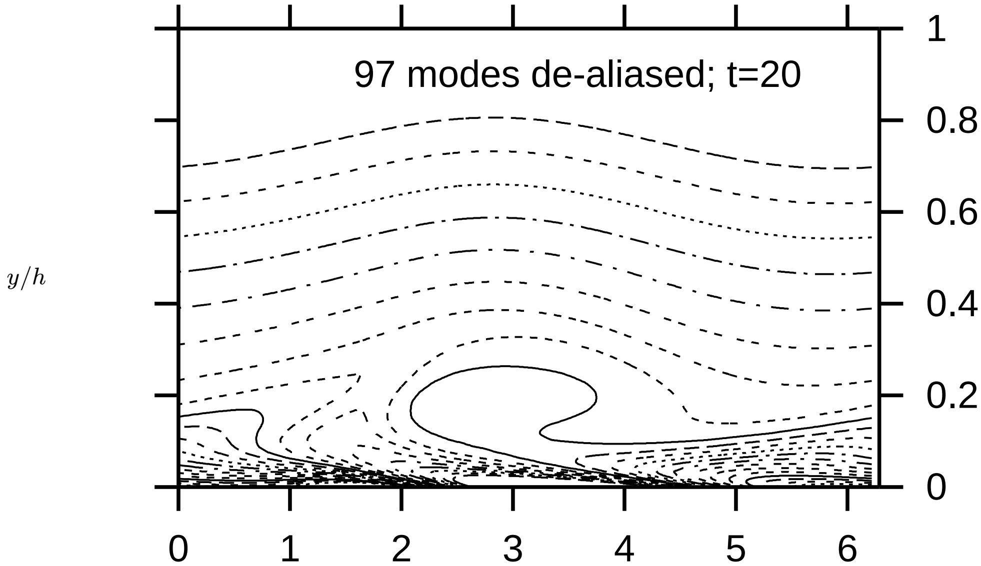

FIGURE 6. Isocontours of spanwise vorticity at values $(-3.5 : .15 : -.5)$ at $t = 20\,h/U_0$ when initialising with the most unstable 2d linear eigenfunction at $Re = 8000$ and using $96 \times 97 \times 32$ modes: de-aliased according to the 3/2-rule.

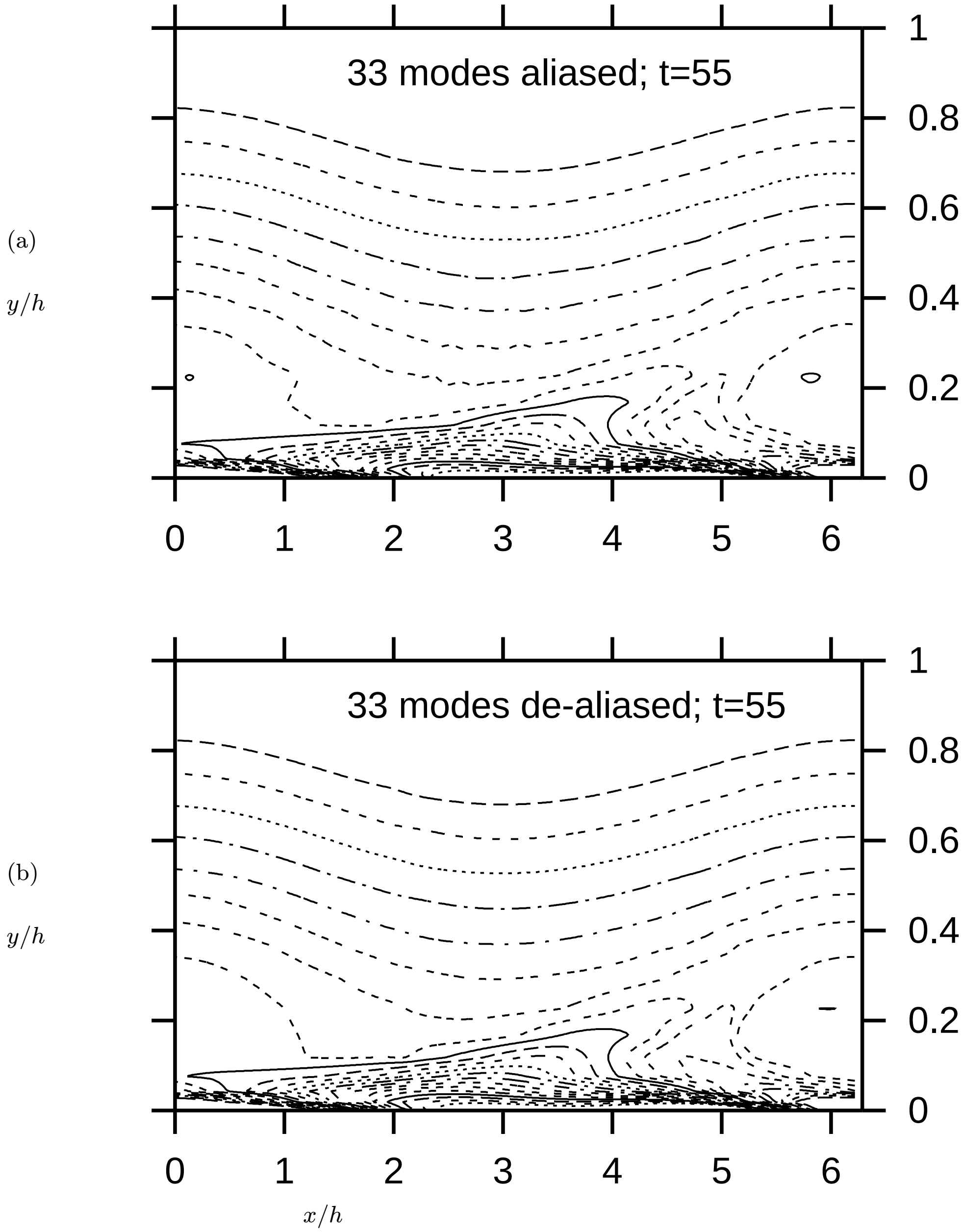

FIGURE 7. Isocontours of spanwise vorticity at values $(-3.5 : .15 : -.5)$ at $t = 55\,h/U_0$ when initialising with the most unstable 2d linear eigenfunction at $Re = 8000$ and using $96 \times 33 \times 32$ modes: (a) aliased Chebyshev modes, (b) de-aliased according to the 3/2-rule.

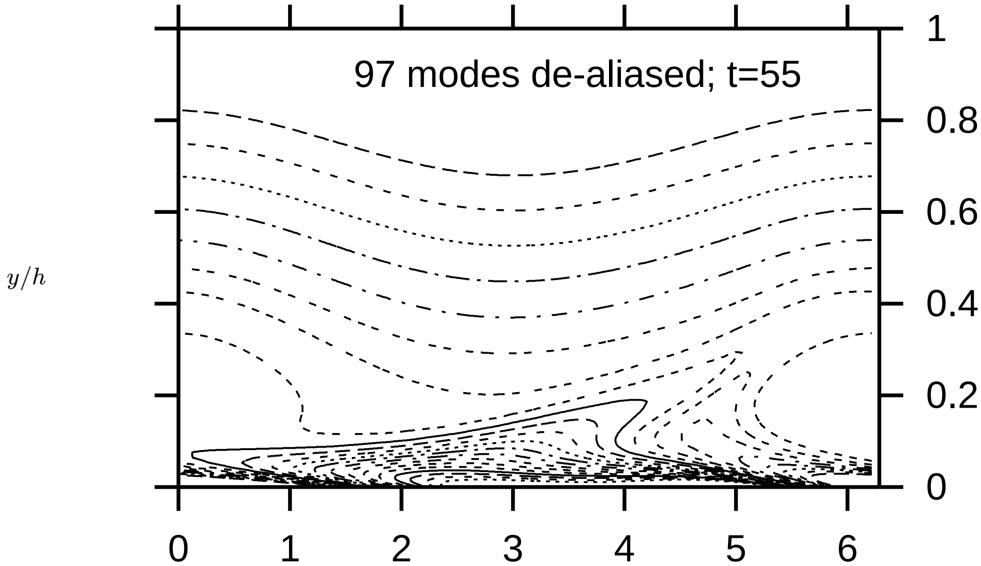

FIGURE 8. Isocontours of spanwise vorticity at values $(-3.5 : .15 : -.5)$ at $t = 55\, h/U_0$ when initialising with the most unstable 2d linear eigenfunction at $Re = 8000$ and using $96 \times 97 \times 32$ modes: de-aliased according to the 3/2-rule.

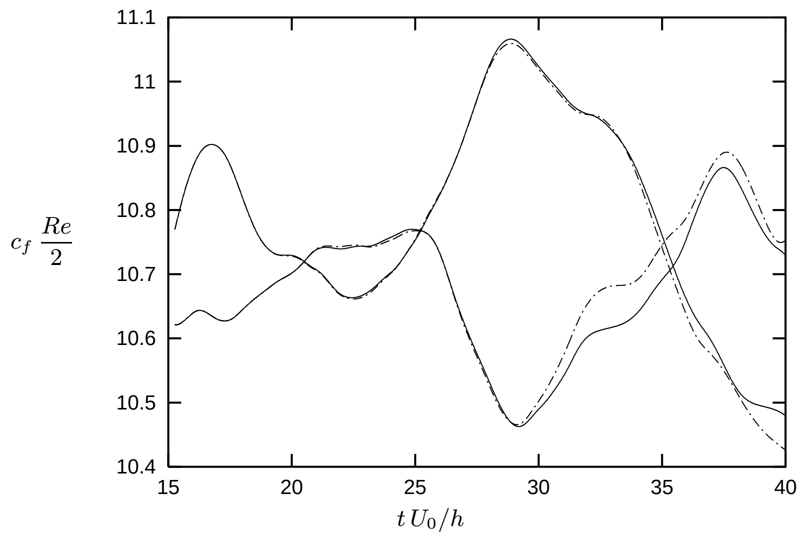

FIGURE 9. Evolution of the plane-averaged wall-friction of both walls during the fully turbulent simulation at $Re = 3250$ having a resolution of $192\times97\times128$ modes. ——— , de-aliased according to the 3/2-rule; —·— , aliased Chebyshev modes.

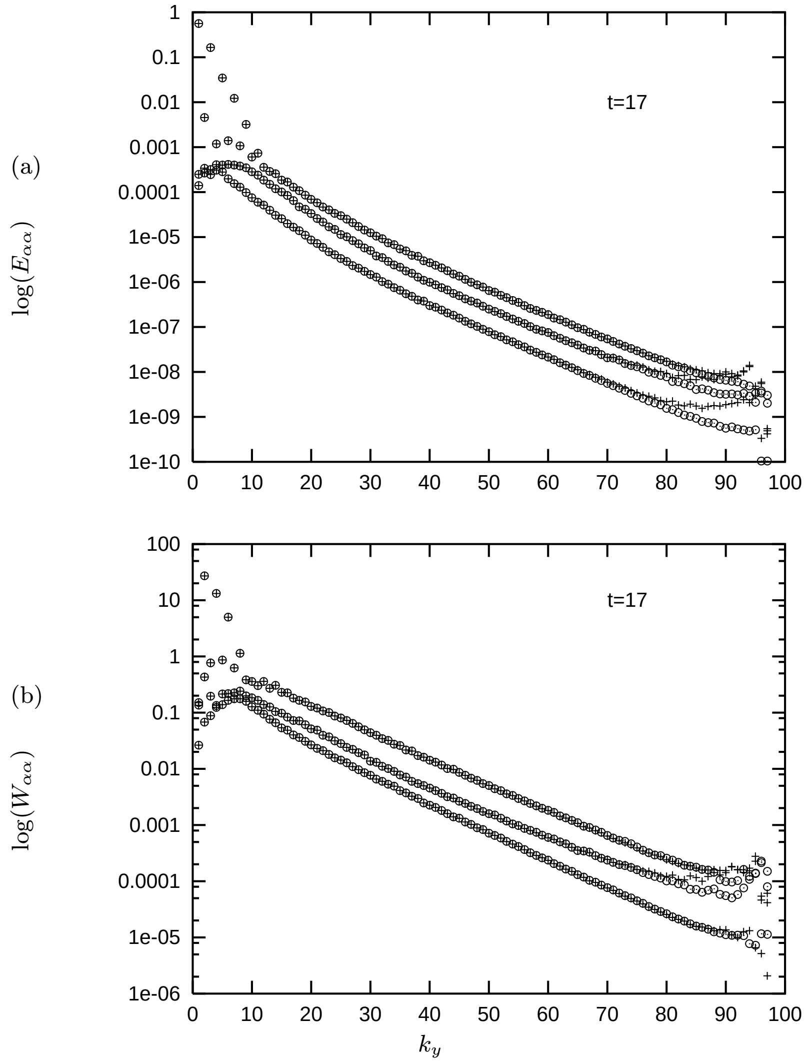

FIGURE 10. Wall-normal spectra of the Chebyshev coefficients of (a) the component energy and (b) the component enstrophy of a fully turbulent simulation at $Re = 3250$ and a resolution of $192 \times 97 \times 128$ modes; $t\,U_0/h = 17$. $+$, aliased Chebyshev modes; $\circ$, de-aliased according to the 3/2-rule.

(a)

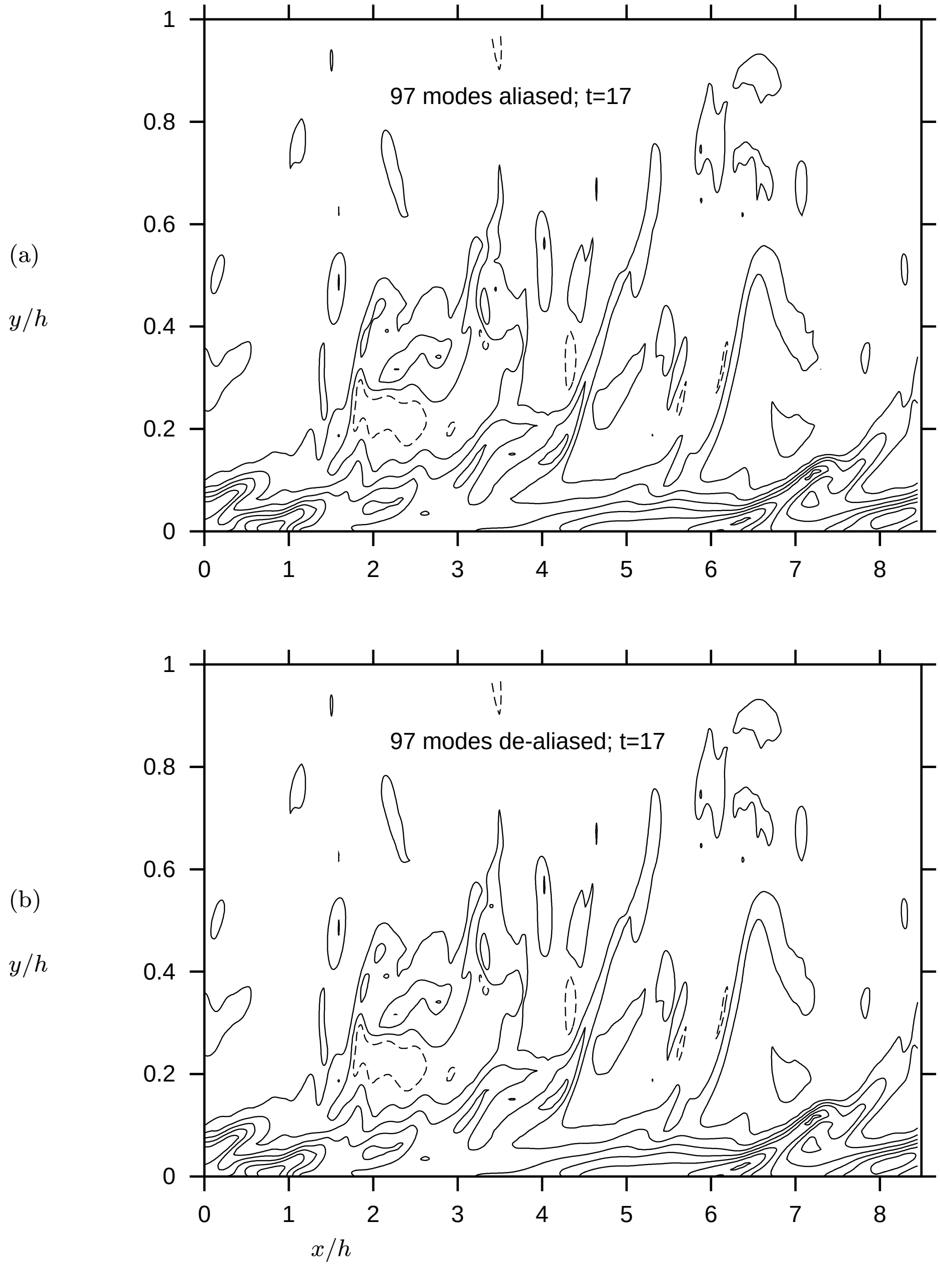

(b)

FIGURE 11. Isocontours of spanwise vorticity at values $(-16 : 2.5 : 1.5)$ at $t = 17\,h/U_0$ of a fully turbulent simulation at $Re = 3250$ and using $192 \times 97 \times 128$ modes: (a) aliased Chebyshev modes, (b) de-aliased according to the 3/2-rule.

(a)

y/h

(b)

y/h

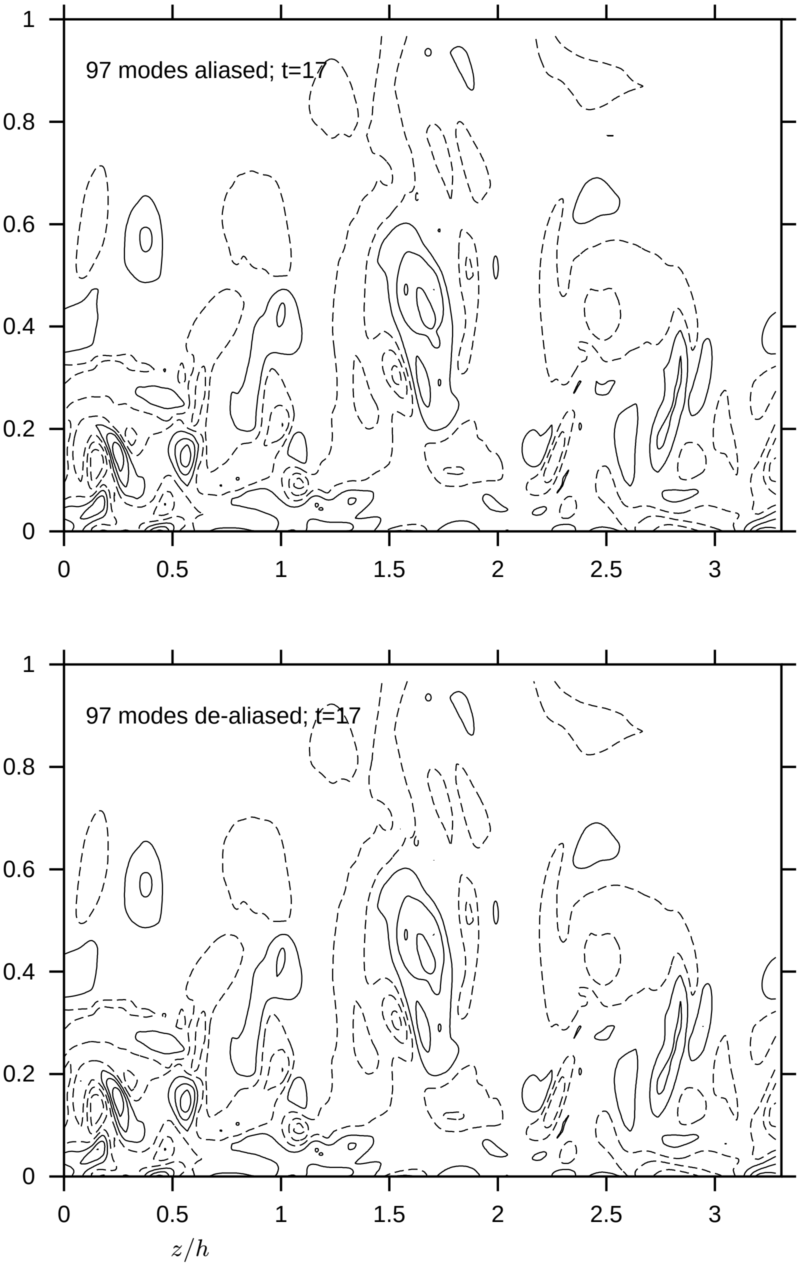

FIGURE 12. Isocontours of streamwise vorticity at values $(-15 : 1.5 : 5)$ at $t = 17\,h/U_0$ of a fully turbulent simulation at $Re = 3250$ and using $192 \times 97 \times 128$ modes: (a) aliased Chebyshev modes, (b) de-aliased according to the 3/2-rule.

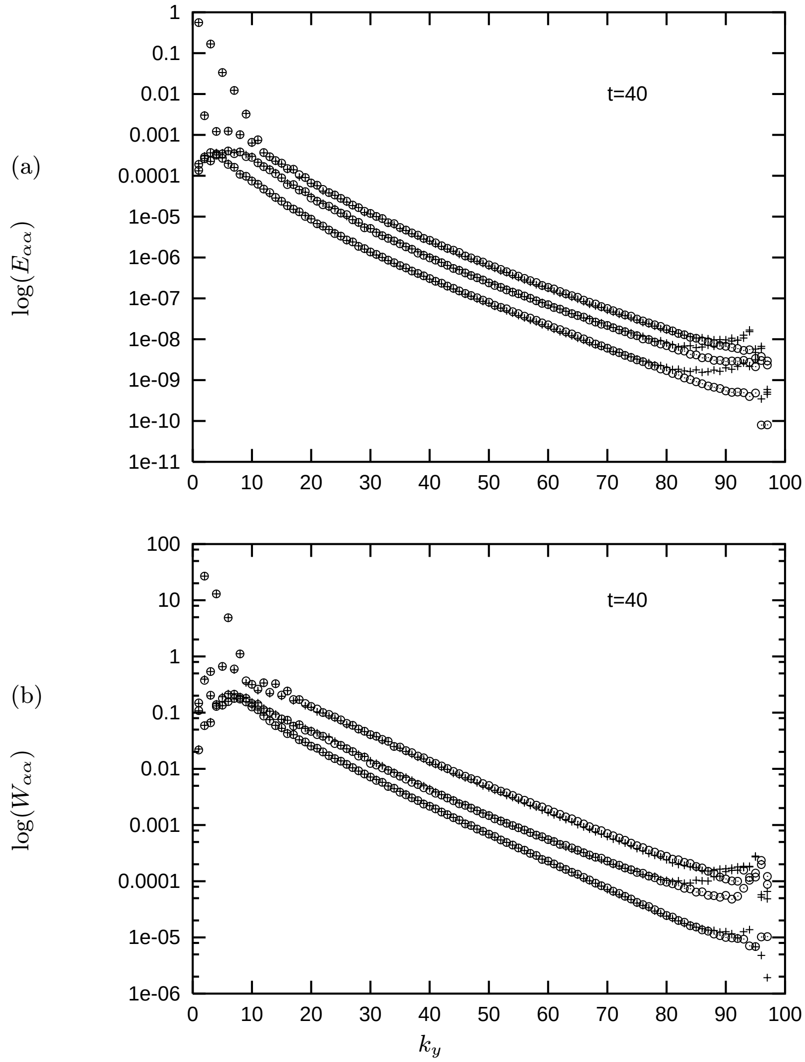

FIGURE 13. Wall-normal spectra of the Chebyshev coefficients of (a) the component energy and (b) the component enstrophy of a fully turbulent simulation at $Re = 3250$ and a resolution of $192 \times 97 \times 128$ modes; $t\,U_0/h = 40$. $+$, aliased Chebyshev modes; $\circ$, de-aliased according to the 3/2-rule.

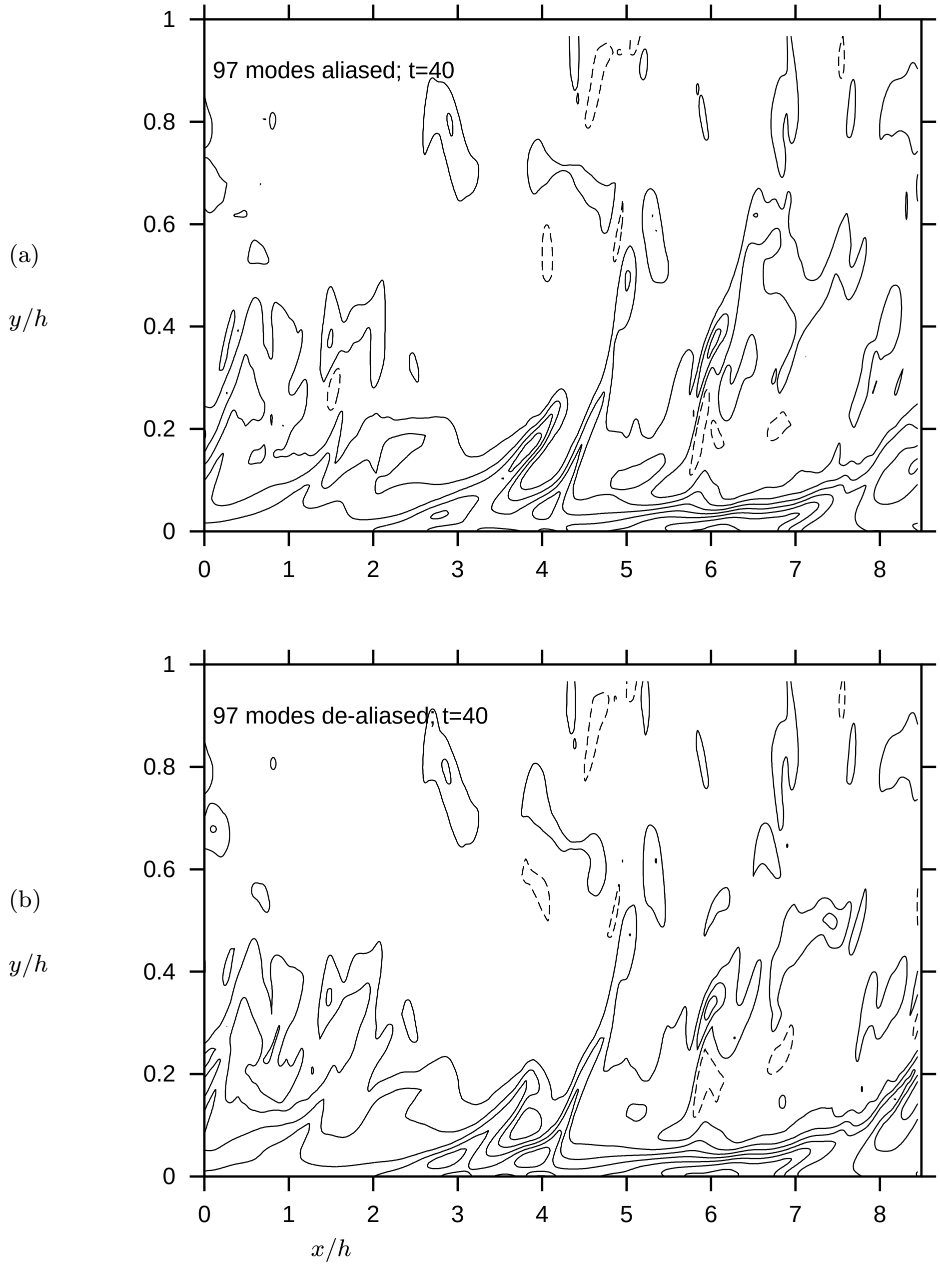

FIGURE 14. Isocontours of spanwise vorticity at values $(-16 : 2.5 : 1.5)$ at $t = 40\,h/U_0$ of a fully turbulent simulation at $Re = 3250$ and using $192 \times 97 \times 128$ modes: (a) aliased Chebyshev modes, (b) de-aliased according to the 3/2-rule.

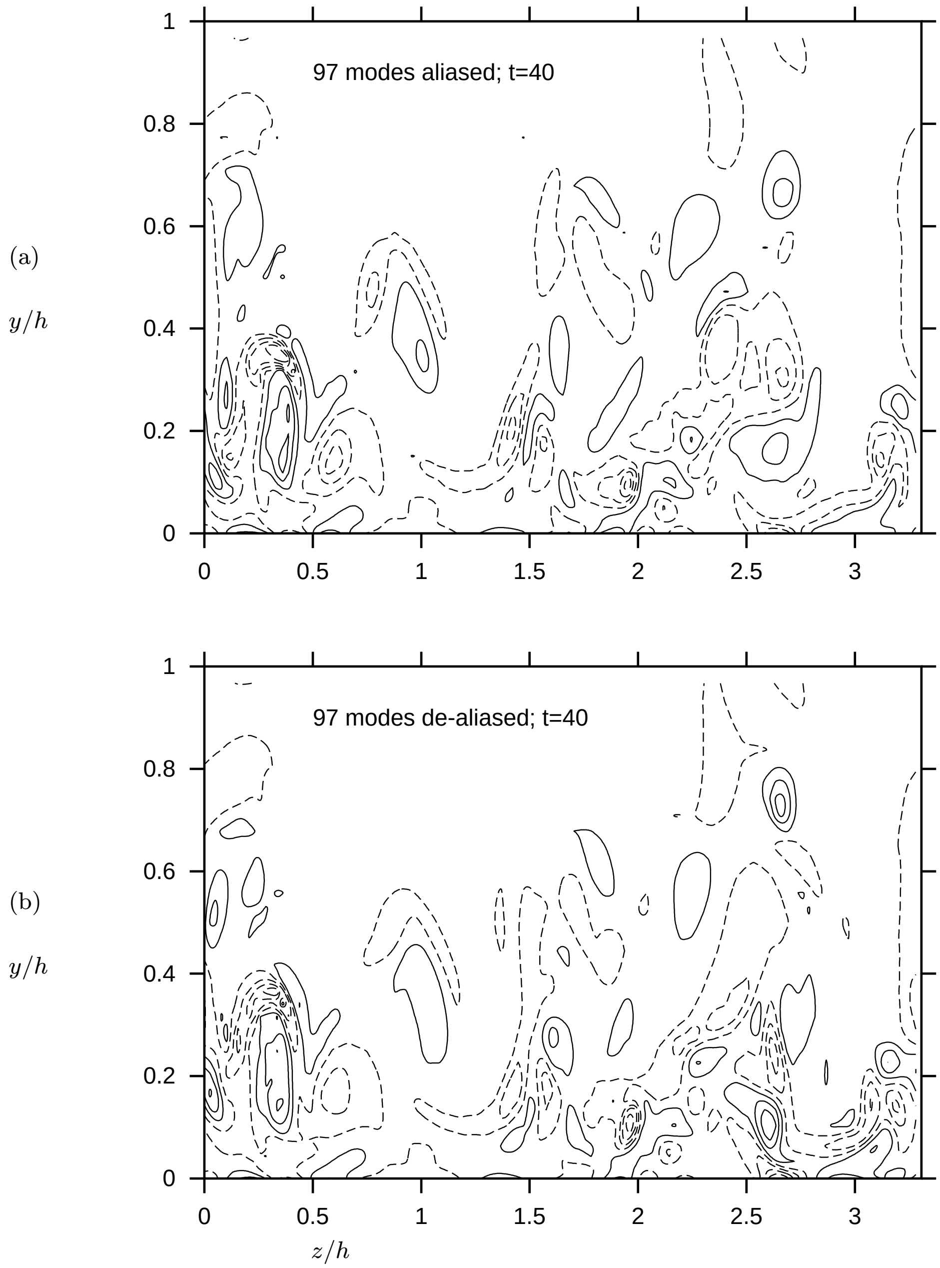

FIGURE 15. Isocontours of streamwise vorticity at values $(-15 : 1.5 : 5)$ at $t = 40\,h/U_0$ of a fully turbulent simulation at $Re = 3250$ and using $192 \times 97 \times 128$ modes: (a) aliased Chebyshev modes, (b) de-aliased according to the 3/2-rule.